Modelling the growth of a PHB producer methanotrophic bacterial strain using a Computational Fluid Dynamic approach: Discontinuous methane feeding strategy

De Crescenzo, C.; Sabbarese, S.; Amabile, C.; Abate, T.; Migliaccio, A.; De Blasio, Cataldo; Chianese, S.; Musmarra, Dino

Published in:
Current Research in Biotechnology

DOI:
10.1016/j.crbiot.2023.100146

Published: 01/01/2023

Document Version
Final published version

Document License
CC BY-NC-ND

Current Research in Biotechnology 6 (2023) 100146

Contents lists available at ScienceDirect

Current Research in Biotechnology

journal homepage: www.elsevier.com/locate/crbiot

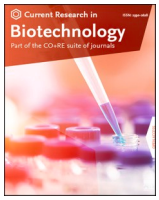

Modelling the growth of a PHB producer methanotrophic bacterial strain using a Computational Fluid Dynamic approach: Discontinuous methane feeding strategy

Carmen De Crescenzo [a], Simona Sabbarese [a], Claudia Amabile [a], Teresa Abate [a], Antimo Migliaccio [a], Cataldo De Blasio [b], Simeone Chianese [a,*], Dino Musmarra [a]

[a] Department of Engineering, University of Campania "Luigi Vanvitelli", Via Roma 29, 81031 Aversa, Italy
[b] Faculty of Science and Engineering, Åbo Akademi University, Rantakatu 2, 65100 Vaasa, Finland

ARTICLE INFO

Keywords:
Mass transfer
Discontinuous methane feeding strategy
Methanotrophic biomass growth modelling
CFD
Poly(3-hydroxybutyrate)

ABSTRACT

Replacing fossil plastic with green and biobased alternatives is one of the most significant challenges of this century. Polyhydroxyalkanoates, more specifically, poly(3-hydroxybutyrate) (PHB), have been found as a very promising alternative to traditional plastics, but currently, they are about 2% of the bioplastics produced. In this work, the growth of a methanotrophic strain belonging to the *Methylocystis* species, a natural producer of poly(3-hydroxybutyrate), was modelled in a bubble column bioreactor fed with methane, considering a discontinuous feeding strategy. Three-dimensional simulations were performed by using a CFD approach. The biomass growth strategy based on the variation of the methane bubble diameter, in a range of 0.003–0.005 m, and the aspect ratio, in the range 5–16, was simulated. Their effects were assessed on the process efficiency and performance in terms of methane fed, biomass and PHB yields. When the bubble diameter was varied, the best performance was achieved at a diameter of 0.005 m with methane fed of 34.2 g, biomass yield of 0.534 $g_{biomass}/g_{CH4}$ and PHB yield of 0.327 g_{PHB}/g_{CH4}. When the aspect ratio was varied, the best performance was achieved at an aspect ratio of 10 with methane fed of 34.9 g, biomass yield of 0.523 $g_{biomass}/g_{CH4}$ and PHB yield of 0.321 g_{PHB}/g_{CH4}. Finally, the estimation of the PHB yield was performed. CFD analysis allowed to verify the absence of death or stagnant zones inside the reactor.

1. Introduction

Plastic pollution represents one of the most widespread environmental problems, which needs a very urgent solution (Bhatia et al., 2021). One approach to face this problem is the progressive substitution of fossil plastic with biodegradable polymers, such as Polyhydroxyalkanoates (PHAs) (Bhatia et al., 2023; Amabile et al., 2023; Amabile et al., 2022). Poly(3-hydroxybutyrate) (PHB), belonging to the PHA family, is one of the most relevant biopolymers with similar properties to thermoplastic (Kim et al., 2023). However, its high costs, which are influenced by the carbon source and the low production yield, the different fermentation methods and extraction procedures induce a lack of marketability (Kumar et al., 2020; Wang et al., 2021). Hence, many studies were carried out focusing on reducing costs: since substrates account for 30–50% of the total process costs (Levett et al., 2016) scientists are strongly intentioned to experiment with low-cost substrates such as coffee grounds (Kang et al., 2023), galactose (Jung et al., 2022), biochar (Bhatia et al., 2022) and lactate (Lee et al., 2022). Among them, methane can be metabolized by methanotrophic bacteria to generate biopolymers (García-Pérez et al., 2018; Rodríguez et al., 2020). For instance, several type II methanotrophic bacteria, such as *Methylocystis parvus* and *Methylocystis hirsuta* produce up to 50 %w/w of PHB when methane is provided as the carbon source and in the absence of nitrogen in the growth medium (Rodríguez et al., 2020; López et al., 2018; Myung et al., 2015). *Methylocystys hirsuta* accumulated 34.6 %w/w of PHB in a 2.5 L bubble column bioreactor (García-Pérez et al., 2018). *Methylocystis* strain generated 51 %w/w of PHB in bioreactors through a double-step process of continuous growth and a discontinuous accumulation (Wendlandt et al., 2001).

Biogas resulting from the anaerobic decomposition of the biodegradable fraction of organic waste is mainly composed of methane (30–70%), carbon dioxide (20–50%) and hydrogen sulphide (<2%)

* Corresponding author.
E-mail address: simeone.chianese@unicampania.it (S. Chianese).

https://doi.org/10.1016/j.crbiot.2023.100146
Received 9 June 2023; Received in revised form 14 September 2023; Accepted 18 September 2023
Available online 19 September 2023

(Rodríguez et al., 2020). Indeed, industrial by-products or waste can represent an opportunity to reduce the cost of PHA production. However, despite the attractiveness of methane as a carbon source, its low solubility limits its concentration in the culture medium, thus leading to low PHB yields. Many solutions have been explored to improve methane-based PHB production yields, including using high-performance bioreactors like bubble columns (Liu et al., 2020). In the design of bubble columns, one of the most critical parameters is the dimension of the column, i.e. the ratio between column height and side basis, defined as aspect ratio (Amabile et al., 2022). In biochemical processes, the aspect ratio varies between 2 and 5 and in industrial processes, the aspect ratio is at least 5 (Kantarci et al., 2005); however, an aspect ratio greater than 5 is preferred because the breakup and coalescence mechanisms reach the steady-state (Amabile et al., 2023; Schügerl et al., 2006). Another critical parameter is the bubble diameter, which affects the gaseous mass transfer (García-Pérez et al., 2018; Amabile et al., 2022). It is important to stress that an optimum reactor design is essential to achieve an effective mass transfer of gas to a liquid, a fundamental criterion for evaluating reactor performance (Chaumat et al., 2005).

CFD simulations have represented a valuable and cost-effective tool to model the gas–liquid fluid dynamics, the interactions, and the mass transfer with reactions, as well as to understand other phenomena occurring in bubble columns and to soften the elevated costs of the experimental procedures (Mühlbauer et al., 2019; Mavaddat et al., 2014). Moradi et al. (Moradi, 2019) simulated the PHB production process starting from natural gas with COMSOL Multiphysics Software. A two-dimensional geometry and an air/water system were used. They aimed to find the optimal conditions of the PHB production process in a bubble bioreactor, investigating the biomass concentration, the gas velocity, the pressure distribution, and the shear stresses in the column.

In this work, the growth of a methanotrophic strain belonging to the *Methylocystis* species, which is a natural producer of PHB, was modelled in a bubble column fed with methane. The growth strategy was approached by varying the methane bubble diameter (d_b) and the reactor geometry in aspect ratio (A), i.e. the ratio between the column height and the side basis, by keeping constant the reactor volume. Their effects on the efficiency and performance of the process were investigated in terms of methane fed and biomass yield. In addition, the assessment of the PHB yield was performed. Since continuous feeding could be ineffective as the consumption of the gaseous carbon sources by the bacterial strains is low, simulations were carried out by performing a discontinuous methane feeding approach: methane was fed to the liquid phase up to the saturation of the working volume; then, the methane feeding was stopped until the whole CH_4 dissolved in the liquid phase was consumed, allowing, at the same time, the continuous biomass growing.

2. Materials and method

2.1. Process modelling

The effects of the variation of d_b (Case study 1) and A (Case study 2) on methane transfer and the production of a methanotrophic strain belonging to *Methylocystis* species, including the assessment of the PHB yield, were investigated by using a Computational Fluid Dynamic approach with chemical reaction. This was implemented in COMSOL Multiphysics® 6 Modeling Software. The physical–chemical properties of the liquid water were defined according to the COMSOL Multiphysics® materials' properties database, while methane was described as a user-defined material.

The methane bubble diameter was varied in a range of 0.003–0.005 m. A working volume (V) of the column, with a square section, of 100 L was considered.

According to the literature, the transition point is found to be independent of the scale if the diameter of the reactor, the height of the column and the aspect ratio exceed the following values (Kumar et al., 1997; Reilly et al., 1994): $A > 5$, $H >$ 1–3 m, $D >$ 0.1–0.2 m. Then, simulations were carried out by considering reactors with the geometry able to avoid the dependency of the transition point by the scale, with A in the range 5–16.

The process was simulated considering two steps: the first concerned the methane transfer from the gas to the liquid up to the saturation of the working volume and the simultaneous bacterial strain growth; the second consisted of the interruption of the CH_4 supply until the bacterial strain completely consumed the CH_4 dissolved in the liquid, according to its growth mechanism. A growth duration of 10 days was simulated by continuously alternating the two steps. The investigated cases are summarised in Table 1.

A three-dimensional geometry (Fig. 1.a) was used, and "fine free triangular" mesh was built in the whole domain by increasing the degree of refinement until the convergence of the solution was obtained. A physics-controlled mesh with 58,746 "domain elements" and 6068 "boundary elements" was defined. The feeding of the methane flow was simulated considering 20 gas spargers represented in Fig. 1.b. Since the mesh refinement degree does not allow a clear mesh display in the entire 3D domain, the mesh is reported only for the top and bottom of the column in Fig. 1.b and 1.c, respectively.

The following boundary conditions were used for the simulations (COMSOL Multiphysics: CFD Module COMSOL User 's Guide., 2019):

- Gas flux for gas and slip for liquid at inlet boundary (Inlet);
- Gas outlet for gas and slip for liquid at the top of column (Outlet);
- No gas flux for gas and no-slip for liquid next to the wall of the column (Wall).

A total methane flow rate, fed to the column through the inlet spargers, of 0.00004 m^3/s was used.

The system temperature and the reference pressure (p_{ref}) were set to 303.15 K and 101,325 Pa, respectively. The bubbly flow model with two phases (i.e. gaseous methane in water) and the *Euler-Euler* approach were used for modelling the CFD multiphase system and for the numerical calculation, respectively. The bubble diameter was used as the input parameter for the simulation process. The solution of the bubble population balance equation allowed the assessment of the surface area. Turbulence in the liquid phase was modelled through standard k-ε model equations with realizability constraints and bubble-induced turbulence production (Ngo and Lim, 2020).

2.1.1. Conservation equations

According to the model proposed, the conservation equations for mass (Eq. (1) and momentum (Eq. (2) reported below were solved for each phase (Besagni et al., 2023). The momentum equations of the phases interact with each other through inter-phase momentum exchange terms. The drag force was only considered, while the added mass force and lift force were neglected in the model for the inter-phase momentum exchange.

$$\frac{\partial(\alpha_k \rho_j)}{\partial t} + \nabla(\alpha_j \rho_j \boldsymbol{U}_j) = S_j \quad (1)$$

Table 1
Summary of the investigated cases.

Case studies		A [-]	d_b [m]
Case study 1	Case 1.a	8	0.003
	Case 1.b	8	0.004
	Case 1.c	8	0.005
Case study 2	**Case 2.a**	5	0.003
	Case 2.b	8	0.003
	Case 2.c	10	0.003
	Case 2.d	16	0.003

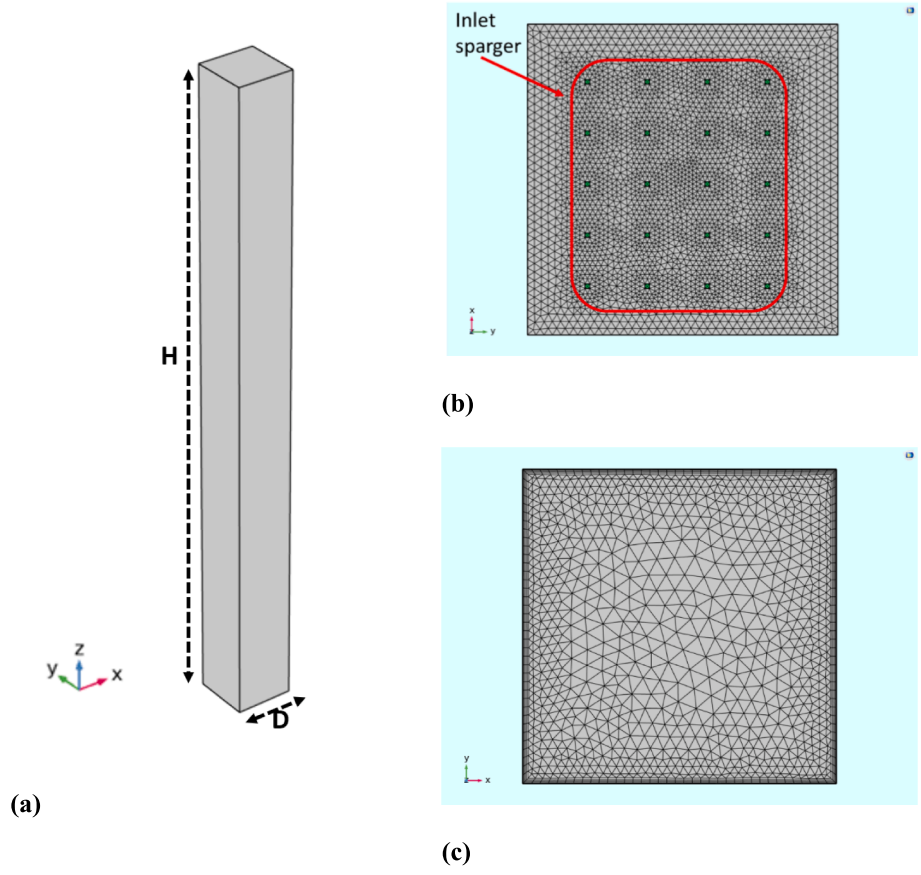

Fig. 1. Schematisation of the bubble column used for the simulation: 3D view (a); mesh of the bottom (b); mesh of the top of the column (c).

$$\frac{\partial(\alpha_j\rho_j\boldsymbol{U}_j)}{\partial t}+\nabla(\alpha_j\rho_j\boldsymbol{U}_j \times \boldsymbol{U}_j) = -\nabla p+\nabla\{\alpha_j\left(\mu_j^v-\mu_j^t\right)\left[\nabla\boldsymbol{U}_j+\left(\nabla\boldsymbol{U}_j\right)^T-\frac{2}{3}\nabla\boldsymbol{U}_jI\right]\}+(\alpha_j\rho_jg)+F_j \quad (2)$$

where:

- the subscript "j" denotes quantities related to the j-th phase (j = L for the liquid phase and j = G for the gas phase);
- α is the volume fraction;
- ρ is the density [kmol/m^3];
- U is the velocity vector [m/s];
- p is the pressure [Pa];
- μ_j^v and μ_j^t are the dynamic and turbulent viscosity of the phase [Pa s], respectively;
- I is the identity tensor; t is the time [s]; g is the gravity vector [m/s^2]
- F_k is any additional volume force [N/m^3];
- S_j is the transfer rate between the gas and liquid phases [mol/(m^3 s)] equal to m_{gl} and -m_{gl} from gas to the liquid and from liquid to the gas phase, respectively (COMSOL Multiphysics: CFD Module COMSOL User 's Guide., 2019).

Using the turbulent kinetic energy, k, as the turbulence model, in combination with the assumption of a negligible gas concentration, the stress tensor contains an extra contribution, and the momentum equations become the following (Mühlbauer et al., 2019; Fletcher et al., 2017):

$$\frac{\partial(\alpha_j\rho_j\boldsymbol{U}_j)}{\partial t}+\nabla(\alpha_j\rho_j\boldsymbol{U}_j \times \boldsymbol{U}_j) = -\nabla p+\nabla\{\alpha_j\left(\mu_j^v-\mu_j^t\right)\left[\nabla\boldsymbol{U}_j+\left(\nabla\boldsymbol{U}_j\right)^T-\frac{2}{3}\nabla\boldsymbol{U}_jI\right]-\frac{2}{3}\alpha_j\rho_jkI\}+(\alpha_j\rho_jg)+F_j \quad (3)$$

2.1.2. Mass transfer model

The concentration of the dissolved gas c [mol/m^3] was calculated through the solution of the following mass transport equation (Mohan et al., 2021). The driving force for transport is convection because it is coupled to a flow field.

$$\frac{\partial c}{\partial t} = -\boldsymbol{U}_l\nabla\bullet c+D_{gas,liquid}\nabla^2c+m_{gl}-K_c \quad (4)$$

where $\boldsymbol{U}_l$ is the liquid velocity vector [m/s]; that can be considered negligible in the case of bubble columns; $D_{gas,liquid}$ is the diffusion coefficient [m^2/s]; m_{gl} is the mass transfer rate from gas to liquid [mol/(m^{3}s)]; and K_c is the source term representing the dissolved gas consumption.

m_{gl} was modelled according to the *Two-film theory* using the following equation (Garcia-Ochoa and Gomez, 2005):

$$m_{gl} = k_La(c^*-c) \quad (5)$$

where k_L is the mass transfer coefficient [m/s]; a is the interfacial area per unit of volume [m^2/m^3]; c* is the equilibrium concentration of gas dissolved in liquid, calculated according to Henry's law (Eq. (6).

$$c^* = \frac{p+p_{ref}}{K_H} \quad (6)$$

where K_H is Henry's constant [Pa l/mol]; p is the operative pressure [Pa]; p_{ref} is the reference pressure [Pa].

The pressure inside the column was calculated according to the following equation (COMSOL Multiphysics: CFD Module COMSOL User 's Guide., 2019):

$$p = (\rho_l \alpha_l + \rho_g \alpha_g) g (H - z) \tag{7}$$

where α is the phase volume fraction; z is z-axis coordinate [m]; and H [m] is the height of the column.

z-axis coordinate is equal to 0 m and H at the bottom and the top of the column, respectively (Fig. 1.a).

The mass transfer coefficient k_L was an input of the model and was calculated as follows:

$$k_L = \frac{Sh D_{gas,liquid}}{d_b} \tag{8}$$

where *Sh* is Sherwood number; $D_{gas,liquid}$ is the diffusivity of gas in liquid [m^2/s].

Sherwood number, *Sh*, for rising large bubbles of gas in liquid as a continuous phase ($d_b > 2$ mm) was calculated according to the Higbie correlation (Eq. (9) (Wang et al., 2020; Calderbank et al., 1970):

$$\mathrm{Sh} = 1.13\, \mathrm{Sc}^{1/2}\, \mathrm{Re}^{1/2} \tag{9}$$

where *Sc* and *Re* are Schmidt and Reynolds non-dimensional numbers, calculated according to Equations (10) and (11), respectively:

$$Sc = \frac{\mu_l}{\rho_l D_{gas,liquid}} \tag{10}$$

$$Re = \frac{d_b \rho_l v_t}{\mu_l} \tag{11}$$

where v_t is the terminal velocity of the bubbles calculated according to the following equation:

$$v_t = \sqrt{\frac{8 F_D}{C_D \pi d_b^2 \rho_l}} \tag{12}$$

In the previous equation, F_D is the drag force calculated according to Eq. (13), and C_D is the drag coefficient, as proposed by Schiller and Naumann (Schiller and Naumann, 1933) (Eq. (14):

$$F_D = \frac{\pi d_b^3 g (\rho_l - \rho_g)}{6} \tag{13}$$

$$C_D = \begin{cases} 24 \dfrac{(1 + 0.15 Re^{0.687})}{Re}, Re \le 1000 \\ 0.44, Re > 1000 \end{cases} \tag{14}$$

The interfacial area per unit of volume, *a*, was calculated according to the following Equation (Eq. (15) (COMSOL Multiphysics: CFD Module COMSOL User 's Guide., 2019):

$$a = (4n\pi)^{\frac{1}{3}} (3\phi_g)^{2/3} \tag{15}$$

where: n is the bubble number density [$1/m^3$]; ϕ_g is the volume fraction of gas [-]. The interfacial area per unit of volume, *a,* varies as a function of time and space inside the column.

2.1.3. Bubble population balance equation

The number density-based population balance equation can be written according to Equation (16) (Shi et al., 2020; Chen et al., 2004).

$$\frac{\partial n}{\partial t} + \nabla \bullet (n \boldsymbol{U}_g) = 0 \tag{16}$$

where U_g is the gas velocity vector [m/s].

2.1.4. Biomass growth reaction and PHB yield

The following biomass growth reaction was used (Rostkowski et al., 2013):

$$\frac{1}{4} CH_4 + \left(\frac{1}{4} + \frac{f_e}{4}\right) O_2 + \frac{f_s}{28} NO_3^- + \left(\frac{29}{28} f_s + f_e - 1\right) H^+ \rightarrow \left(\frac{1}{4} - \frac{5 f_e}{28}\right) CO_2 + \left(\frac{f_e}{2} + \frac{11 f_s}{28}\right) H_2O + \left(\frac{f_s}{28}\right) C_5 H_7 O_2 N \tag{17}$$

with f_e equal to 0.48 and f_s equal to 0.52, thus resulting in 0.074 mol of biomass produced per mole of methane. A zero-order kinetic reaction was considered (Amabile et al., 2022). This kinetic reaction order is coherent with experimental data reported in the scientific literature (Myung et al., 2015), which were used for the assessment of the kinetic constant, K_k, equal to 0.000106 kmol/m^3h. The following equation was used to model the kinetic reaction for biomass growth:

$$R_{C\_BIOM} = K_k * 0.074 \tag{18}$$

It is worth highlighting that the mass transfer of methane was considered the limiting (slow) step of the process. Therefore, the simulation process was exclusively focused on methane. According to the literature, a slow reaction was considered, and the mass transfer was not assumed to be chemically enhanced, as previously assessed (Amabile et al., 2022) and in agreement with the scientific literature (Garcia-Ochoa et al., 2010).

The PHB yield was assessed based on the scientific literature data. In particular, for *Methylocystis* species, a PHB content equal to 38 %w/w, related to the PHB amount in the total solids (i.e. PHB + bacterial biomass), was reported (García-Pérez et al., 2018; Myung et al., 2015). It is worth highlighting that the PHB content specified above, used for the assessment of the PHB production in this manuscript, is an average value observed for the genus *Methylocystis* and represents the final PHB content at the end of the accumulation process without nutrients (i.e. nitrogen).

The above-mentioned hypothesis and assumption are summarized in Table 2.

The biomass yield, i.e. the biomass produced per unit of CH_4 fed, and the PHB yield, i.e. PHB produced per unit of CH_4 fed, and the CH_4 fed, were assessed as indicators of the process performance.

3. Results and discussion

3.1. Discontinuous methane feeding strategy

The simulations were carried out by the discontinuous feeding of the methane. To better explain the methane feeding and biomass growth strategies, as an example, the trend of the dissolved CH_4 and the cumulative biomass concentrations for case 1.a is reported in Fig. 2. The methane was fed to the liquid phase up to the saturation of the working volume, i.e. the dissolved CH_4 concentration increased till the saturation (Table 4). Afterwards, the methane feeding was interrupted until the CH_4 dissolved was consumed by the biomass growth. Then, methane was fed again up to column saturation, and the feeding cycle was repeated for a simulation time of 10 days, allowing the continuous biomass growth for the duration considered. It is worth highlighting that with the proposed approach, the dissolved CH_4 and the fed CH_4 for the biomass growth correspond.

This strategy was implemented to save methane since continuous feeding could result in ineffective, as the consumption of the gaseous substrate is low, as reported in the scientific literature (García-Pérez et al., 2018; Rodríguez et al., 2020).

3.2. Effects of the variation of the methane bubble diameter d_b

The effect of the variation of d_b on *Re*, *Sc*, *Sh* and k_L, by keeping

Table 2
Modelling condition for the simulation of the biological phase.

Step	Reaction order	Limiting step	Reaction regime	Ref
Biomass growth	Zero (reaction rate constant value = 0.000106 kmol/m^{3}h)	Methane mass transfer	Slow	(Myung et al., 2015; Amabile et al., 2022; Garcia-Ochoa et al., 2010)
PHB accumulation	PHB = 38% w/w			(García-Pérez et al., 2018; Myung et al., 2015)

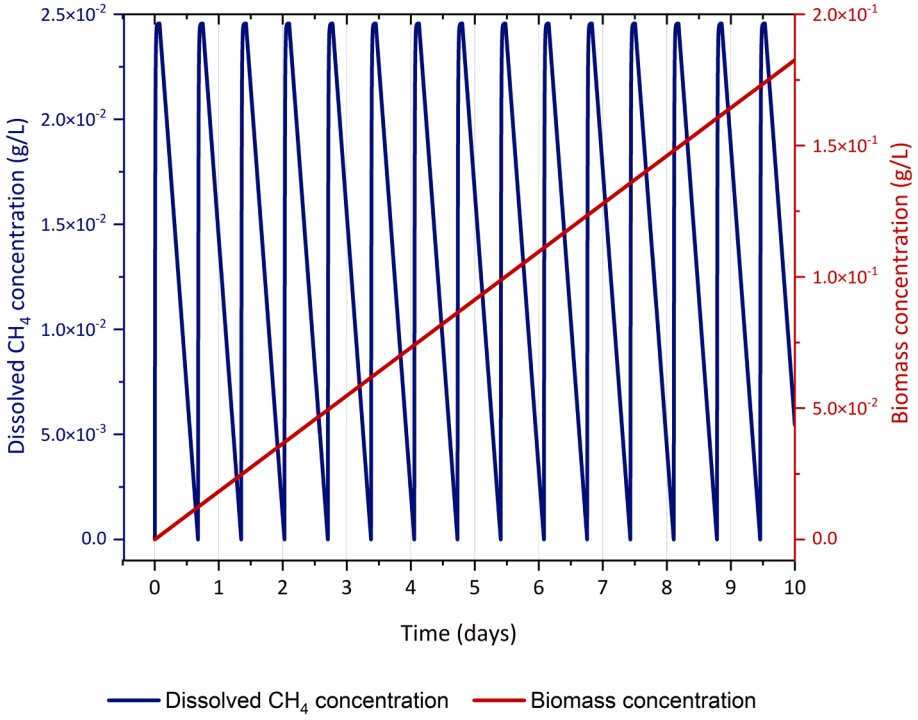

Fig. 2. Dissolved CH_4 and biomass concentrations as a function of the simulated growth time for the case 1.a.

Table 3
Values of *Re*, *Sc*, *Sh* and k_L calculated for the different values of d_b investigated.

	Case 1.a	Case 1.b	Case 1.c
d_b [m]	0.003	0.004	0.005
Re [-]	1,004	1,546	2,161
Sc [-]	598	598	598
Sh [-]	876	1,087	1,285
k_L [m/s]	0.00044	0.00040	0.00038

constant *A* and *V*, is shown in Table 3. Since *Re* was higher than 1000 for all the cases analysed, C_D was set to 0.44 (Eq. (14).

The mass transfer coefficient slightly decreased with increasing d_b (Painmanakul et al., 2009). This trend was confirmed by the saturation time of the bubble column (Table 4), which increased by increasing d_b, passing from 6,340 s with d_b equal to 0.003 mm, to 9,950 s with d_b equal to 0.005 m.

The methane saturation concentration, c^*, was slightly affected by the variation of the bubble diameter since it mainly depends on the pressure inside the column, which, in turn, is a function of the liquid height of the column. Moreover, since the aspect ratio *A* was kept constant at 8, i.e. the height of the liquid was not varied, nearly the same value of c^* for cases 1.a, 1.b and 1.c was assessed (Table 4).

Table 4
Values of saturation time, c* and operative pressure for the different values of d_b investigated.

	Case 1.a	Case 1.b	Case 1.c
d_b [m]	0.003	0.004	0.005
Saturation time [s]	6,340	8,000	9,950
c^* [g/l]	0.0246	0.0244	0.0243
Operative pressure [Pa]	9,068		

The trend of dissolved methane and the biomass yield during the first methane feeding cycle is sketched in Fig. 3. The first methane feeding cycle lasted less than one day, about 60,000 s, for all the cases simulated. As shown, the lower the d_b, the lower the time required for the whole consumption of the methane dissolved, influencing the total number of methane feeding cycles, which decreased by increasing d_b (Table 5); while the time for achieving the maximum biomass yield seems to be slightly affected by the methane bubble diameter. The trend of CH_4 consumption after saturation presents the same slope, being the biomass growth reaction the same (Eq. (18).

The number of methane feeding cycles, the total CH_4 fed, the average amount of CH_4 fed for unit of reactor volume and time, the biomass yield and the PHB yield were assessed as a function of d_b and reported in Table 5. At the simulated growth time of 10 days, the biomass yield and the PHB yield varied in the range of 0.502–0.534 $g_{biomass}/g_{CH4}$ and 0.307–0.327 g_{PHB}/g_{CH4}, respectively. The total methane dissolved in the liquid decreased by increasing d_b. These results can be explained by considering the effect of d_b on the mass transfer (the lower the d_b, the higher the k_L) and the saturation time (the lower the d_b, the lower the saturation time), which also reduces the number of feeding cycles over 10 days. Biomass and PHB yields show an opposite trend with respect to the methane dissolved, as the higher the bubble diameter, the higher the

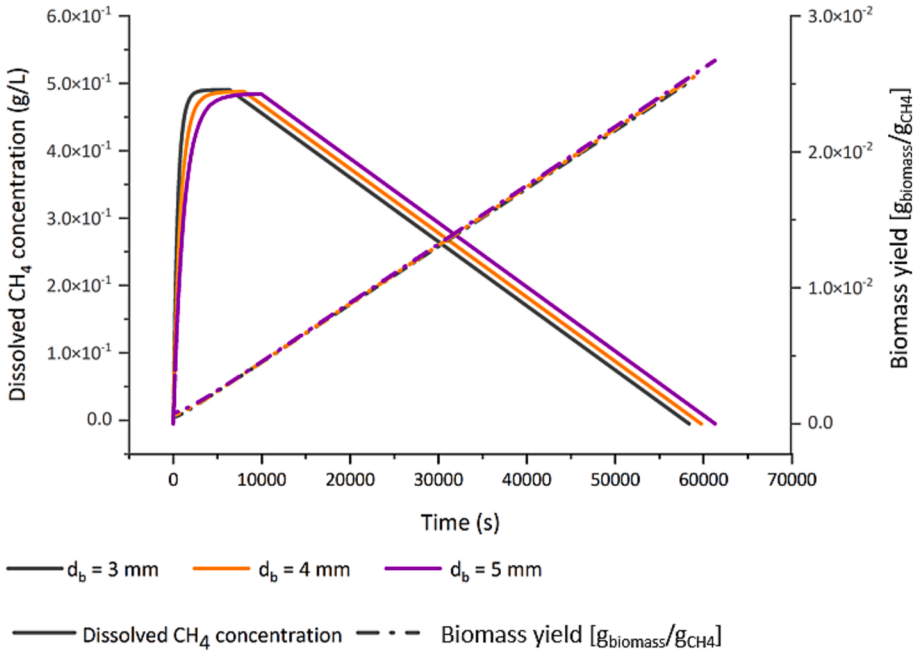

Fig. 3. Dissolved CH_4 concentration (filled lines) and biomass yield (dash-dot-dot lines) for different values of d_b investigated.

Table 5
Number of methane feeding cycles, CH_4 fed, biomass and PHB yields at a simulated growth time of 10 days for different values of d_b investigated.

	Case 1.a	Case 1.b	Case 1.c
d_b [m]	0.003	0.004	0.005
Number of methane feeding cycles	14.805	14.468	14.092
CH_4 fed [g]	36.4	35.3	34.2
Average CH_4 fed [g/m^3 h]	1.51	1.47	1.42
Biomass yield [$g_{biomass}/g_{CH4}$]	0.502	0.517	0.534
PHB yield [g_{PHB}/g_{CH4}]	0.307	0.317	0.327

biomass yield and the PHB yield.

According to the assumptions made, the biomass growth strategy based on the variation of the bubble diameter highlighted that the increase in the mass transfer is ineffective for the growth of the biomass and the production of PHB.

Biomass concentration after a growth time of 10 days and PHB productivity reported in this work, ≅ 0.18 g/L and ≅ 11 g/m^3 d, respectively, are comparable with the ones achieved by Rodríguez et al. (Rodríguez et al., 2023), equal to ≅ 0.5 g/L and ≅ 20 g/m^3 d, respectively. According to the scientific literature, the growth of methanotrophic biomass, such as *Methylocystis* species, and the production of PHB with a content of about 30 %w/w, requires a methane feeding in the range from ≅ 10 g/m^3 h to ≅ 200 g/m^3 h (García-Pérez et al., 2018; Rodríguez et al., 2020). In terms of CH_4 fed, our results report an average value from a minimum of 1.42 g/m^3 h (d_b = 0.005 m) to a maximum of 1.51 g/m^3 h (d_b = 0.003 m), highlighting that the innovative feeding strategy proposed may allow the reduction of methane feeding of 1–2 orders of magnitude, saving the utilization of this resource.

3.3. Effects of the variation of the aspect ratio a

The effect of the variation of A on the saturation conditions of the bubble column by keeping constant d_b and V, is shown in Table 6. It is worth highlighting that mass transfer is not affected by the variation of A, but it strongly depends on the bubble diameter. Therefore, since d_b was kept constant at the value of 0.003 m, Re, Sc, Sh, and K_L were equal to 1,004, 594, 876 and 0.00044 m/s, respectively. Moreover, since Re was higher than 1,000, C_D was set equal to 0.44 (Eq. (14). Simulations of the Case 2 were carried out by using the diameter of 0.003 m because it minimizes the saturation time.

Table 6
Values of saturation time, c* and operative pressure for the different values of A investigated.

	Case 2.a	Case 2.b	Case 2.c	Case 2.d
A [-]	5	8	10	16
Saturation time [s]	7,820	6,340	8,890	7,840
c^* [g/L]	0.0239	0.0246	0.0249	0.0258
Operative pressure [Pa]	6,631	9,068	10,518	14,373

The saturation time of the bubble column is not linearly dependent upon A, being equal to 7,820 s, 6,340 s, 8,890 s, and 7,840 s for A values of 5, 8, 10 and 16, respectively (Table 6). On the other hand, the methane saturation concentration, c^*, which depends on the pressure, and in turn, on the gas hold-up and the liquid height (according to Eq.6), increased with A passing from 0.0239 g/L to 0.0258 g/L. The average values of the operative pressure inside the bubble column are reported in Table 6 to highlight the effect of this parameter on the saturation conditions, i.e. the higher the aspect ratio, the higher the operative pressure, and the higher the methane saturation concentration.

The trend of dissolved methane and biomass yield during the first methane feeding cycle is reported in Fig. 4. The first methane feeding cycle lasted less than one day, about 60,000 s, for all the cases simulated. According to this trend, the lower the A, the lower the time required for the whole consumption of the methane dissolved, and the lower the time for the maximum biomass yield. Consequently, the total number of methane feeding cycles is reduced by increasing A (Table 7). CH_4 reduction after saturation presents the same slope, being the biomass growth reaction the same (Eq. (18).

The number of methane feeding cycles, the total CH_4 fed, the average amount of CH_4 fed for unit of reactor volume and time, the biomass yield and the PHB yield were assessed as a function of A and reported in Table 7.

At the simulated growth time of 10 days, the highest biomass and PHB yields were evaluated for the aspect ratio equal to 10, to which the lowest total methane fed corresponds. The biomass yield and the PHB

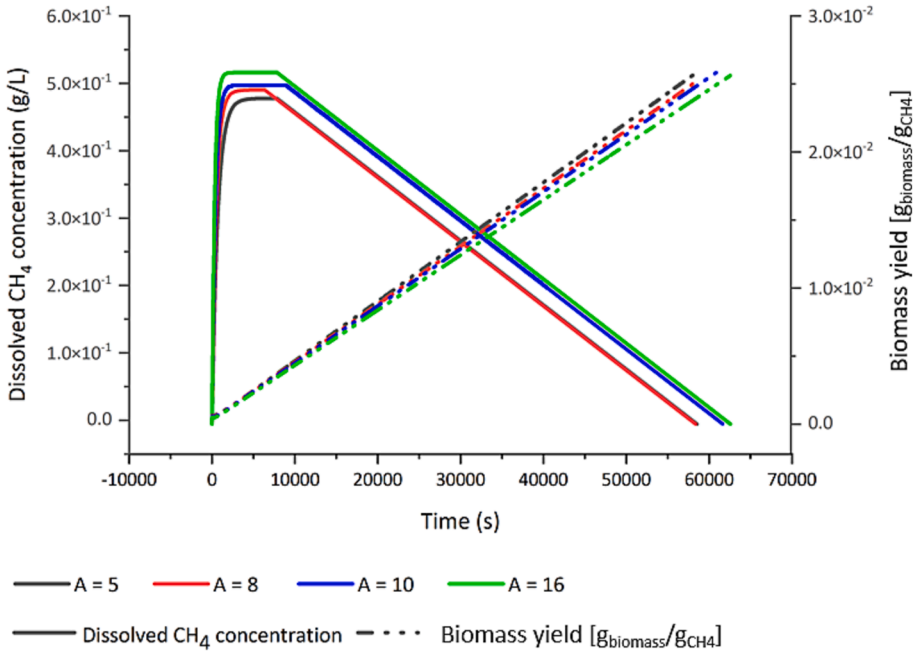

Fig. 4. Dissolved CH_4 concentration (filled lines) and biomass yield (dash-dot-dot lines) for different values of *A* investigated.

Table 7
Number of methane feeding cycles, CH_4 fed, biomass and PHB yields at a simulated growth time of 10 days for different values of *A* investigated.

	Case 2.a	Case 2.b	Case 2.c	Case 2.d
A **[-]**	5	8	10	16
Number of methane feeding cycles	14.764	14.805	14.012	13.811
CH_4 fed [g]	35.4	36.4	34.9	35.7
Average CH_4 fed [g/m^3 d]	1.47	1.51	1.45	1.48
Biomass yield [$g_{biomass}/g_{CH4}$]	0.517	0.502	0.523	0.512
PHB yield [g_{PHB}/g_{CH4}]	0.316	0.307	0.321	0.314

yield varied in the range of 0.502–0.523 $g_{biomass}/g_{CH4}$ and 0.307–0.321 g_{PHB}/g_{CH4}, respectively. It is worth highlighting that, for the aspect ratio considered, these values are one order of magnitude higher with respect to data available in literature when a methane continuous feeding approach is used and 1–3 times higher than the literature findings when high gas recycling ratios are used (García-Pérez et al., 2018; Rodríguez et al., 2020; Amabile et al., 2022).

According to the assumptions made, the biomass growth strategy based on the aspect ratio variation highlighted that the reactor geometry is effective for the growth of the biomass and the production of PHB.

The results reported in Table 7 confirm that the biomass concentration after a growth time of 10 days and PHB productivity reported in this work are comparable with the ones achieved by Rodríguez et al. (Rodríguez et al., 2023). Moreover, regarding the average amount of CH_4 fed, the results point out that the innovative feeding strategy proposed may allow to save methane, reducing the feeding of 1–2 orders of magnitude (García-Pérez et al., 2018; Rodríguez et al., 2020).

3.4. Gas phase velocity distribution

The gas velocity distribution inside the reactor and at the inlet section at three different times (1,000 s, 2,000 s and 3,000 s) before the saturation of the column for case 2.d, which showed the highest production of biomass among the cases simulated, is reported in Fig. 5. A higher velocity can be found in the lower part of the column with a non-uniform distribution of the gas velocity due to the spargers at the bottom. Gas velocity resulted more constant but lower at the top of the column, where the influence of the gas sparger was not perceived. At the top of the column, the gas velocity varied in the range of 0.288–0.295 m/s and matched with the terminal velocity of the bubble, calculated according to equation (12). In addition, CFD simulations show the absence of death or stagnant zones inside the reactor, which favour the transfer of methane and the production of biomass.

4. Conclusions

This work deals with modelling the growth of a PHB producer Methanotrophic bacterial strain using a Computational Fluid Dynamic approach, proposing an innovative discontinuous methane feeding strategy. Moreover, the bubble diameter and aspect ratio variations were simulated, and their effects on the process performance were assessed. The mass transfer coefficient increased with decreasing bubble diameter, but the aspect ratio variation did not affect it. Nevertheless, the increase in mass transfer seems to be ineffective for the growth of biomass and the production of PHB. At the same time, the reactor geometry is effective on the biomass and PHB yields. The proposed methane feeding strategy is valuable, as it may reduce methane feeding by 1–2 orders of magnitude. Fluid-dynamics analysis allows to determine the presence of death or stagnant zones.

Even if promising results are reported in this study, further CFD studies and experimental investigations are required to validate the proposed approach.

CRediT authorship contribution statement

Carmen De Crescenzo: Methodology, Software, Writing – original draft. **Simona Sabbarese:** Investigation, Software, Writing – original draft. **Claudia Amabile:** Validation. **Teresa Abate:** Visualization. **Antimo Migliaccio:** Visualization. **Cataldo De Blasio:** Writing – review & editing. **Simeone Chianese:** Conceptualization, Writing – review & editing. **Dino Musmarra:** Supervision, Funding acquisition.

Declaration of Competing Interest

The authors declare that they have no known competing financial

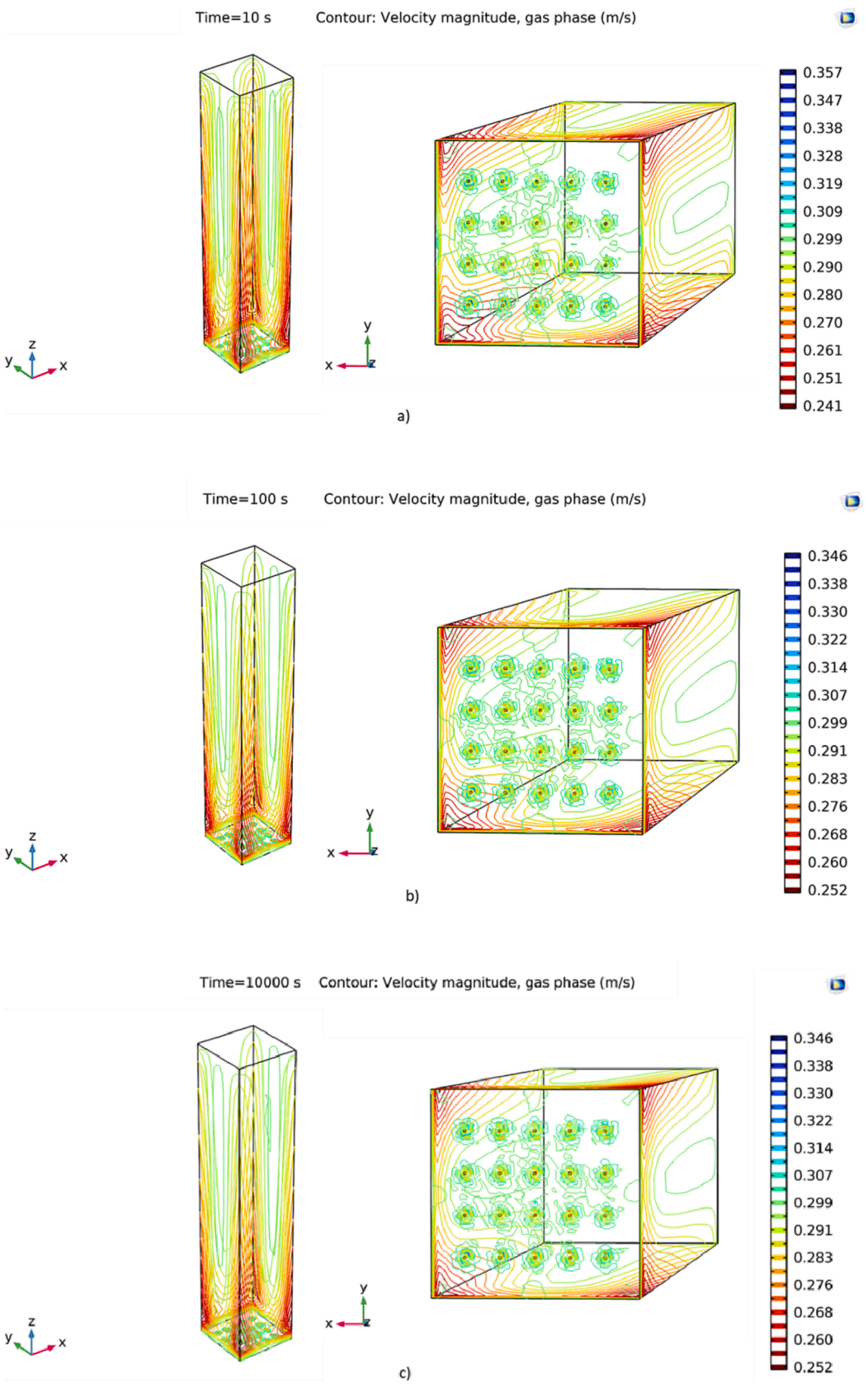

Fig. 5. Gas phase velocity distribution into the reactor and at the inlet section at three different times: 10 s (a); 100 s (b); 1,000 s (c).

interests or personal relationships that could have appeared to influence the work reported in this paper.

Data availability

Data will be made available on request.

Acknowledgement

This work has been supported by the Government of Italy Ministry of Economic Development through the "Fondo per la Crescita Sostenibile – Sportello "Agrifood" PON I&C 2014-2020", di cui al D.M. 5 marzo 2018 Capo III. Prog. n. F/200125/01-03/X45. Authors would like to thank VALERE "VAnviteLli pEr la RicErca" PROGRAMME by the University of Campania Luigi Vanvitelli.

References

Amabile, C., Abate, T., De Crescenzo, C., Sabbarese, S., Migliaccio, A., Chianese, S., Musmarra, D., 2022. Poly(3-hydroxybutyrate) production from methane in bubble column bioreactors: process simulation and design optimization. N. Biotechnol. 70, 39–48.

Amabile, C., Abate, T., De Crescenzo, C., Sabbarese, S., Muñoz, R., Chianese, S., Musmarra, D., 2022. Sustainable process for the production of poly(3-hydroxybutyrate- *Co* -3-hydroxyvalerate) from renewable resources: A simulation study. ACS Sustain. Chem. Eng. 10, 14230–14239.

Amabile, C., Abate, T., De Crescenzo, C., Muñoz, R., Chianese, S., Musmarra, D., 2023. An innovative and sustainable process for producing poly(3-hydroxybutyrate-co-3-hydroxyvalerate): simulating volatile fatty acid role and biodegradability. Chem. Eng. J. 473, 145193.

Amabile, C., Abate, T., Chianese, S., Musmarra, D., Muñoz, R., 2023. the co-conversion of methane and mixtures of volatile fatty acids into poly(3-hydroxybutyrate-co-3-hydroxyvalerate) expands the potential of an integrated biorefinery. Bioresour. Technol. 387, 129699.

Besagni, G., Varallo, N., Mereu, R., 2023. Computational fluid dynamics modelling of Two-Phase bubble columns: A comprehensive review. fluids 8, 91.

Bhatia, S.K., Otari, S.V., Jeon, J.-M., Gurav, R., Choi, Y.-K., Bhatia, R.K., Pugazhendhi, A., Kumar, V., Rajesh Banu, J., Yoon, J.-J., et al., 2021. Biowaste-to-bioplastic (polyhydroxyalkanoates): Conversion technologies, strategies, challenges, and perspective. Bioresour. Technol. 326, 124733.

Bhatia, S.K., Gurav, R., Kim, B., Kim, S., Cho, D.-H., Jung, H., Kim, Y.-G., Kim, J.-S., Yang, Y.-H., 2022. Coproduction of exopolysaccharide and polyhydroxyalkanoates from sphingobium yanoikuyae BBL01 using biochar pretreated plant biomass hydrolysate. Bioresour. Technol. 361, 127753.

Bhatia, S.K., Hwang, J.H., Oh, S.J., Kim, H.J., Shin, N., Choi, T.-R., Kim, H.-J., Jeon, J.-M., Yoon, J.-J., 2023. Yang y-H: **Macroalgae as a source of sugar and detoxifier biochar for polyhydroxyalkanoates production by halomonas sp. YLGW01 under the unsterile condition**. Bioresour. Technol. 384, 129290.

Calderbank, P.H., Johnson, D.S.L., Loudon, J., 1970. Mechanics and mass transfer of single bubbles in free rise through some newtonian and non-Newtonian liquids. Chem. Eng. Sci. 25, 235–256.

Chaumat, H., Billet-Duquenne, A.M., Augier, F., Mathieu, C., Delmas, H., 2005. Mass transfer in bubble column for industrial conditions—effects of organic medium, gas and liquid flow rates and column design. Chem. Eng. Sci. 60, 5930–5936.

Chen, P., Sanyal, J., Dudukovic, M.P., 2004. CFD modeling of bubble columns flows: implementation of population balance. Chem. Eng. Sci. 59, 5201–5207.

COMSOL Multiphysics: *CFD Module COMSOL User 's Guide*. 2019.

Fletcher, D.F., McClure, D.D., Kavanagh, J.M., Barton, G.W., 2017. CFD simulation of industrial bubble columns: Numerical challenges and model validation successes. App. Math. Model. 44, 25–42.

Garcia-Ochoa, F., Gomez, E., 2005. Prediction of gas-liquid mass transfer coefficient in sparged stirred tank bioreactors. Biotechnol. Bioeng. 92, 761–772.

Garcia-Ochoa, F., Gomez, E., Santos, V.E., Merchuk, J.C., 2010. Oxygen uptake rate in microbial processes: An overview. Biochem. Eng. J. 49, 289–307.

García-Pérez, T., López, J.C., Passos, F., Lebrero, R., Revah, S., Muñoz, R., 2018. Simultaneous methane abatement and PHB production by methylocystis hirsuta in a novel gas-recycling bubble column bioreactor. Chem. Eng. J. 334, 691–697.

García-Pérez, T., López, J.C., Passos, F., Lebrero, R., Revah, S., Muñoz, R., 2018. Optimization of CH4 removal from diluted emissions and continuous PHB production by methylocystis hirsuta: towards GHG biorefineries. Chem. Eng. Trans. https://doi.org/10.3303/CET1868074.

Jung, H.J., Kim, S.H., Cho, D.H., Kim, B.C., Bhatia, S.K., Lee, J., Jeon, J.-M., Yoon, J.-J., Yang, Y.-H., 2022. Finding of novel galactose utilizing Halomonas sp. YK44 for polyhydroxybutyrate (PHB) production. *Polymers (Basel)* 2022, 14:5407.

Kang, B.-J., Jeon, J.-M., Bhatia, S.K., Kim, D.-H., Yang, Y.-H., Jung, S., Yoon, J.-J., 2023. Two-stage bio-hydrogen and polyhydroxyalkanoate production: upcycling of spent coffee grounds. Polymers (Basel) 15, 681.

Kantarci, N., Borak, F., Ulgen, K.O., 2005. Bubble column reactors. Process Biochem. 40, 2263–2283.

Kim, B., Oh, S.J., Hwang, J.H., Kim, H.J., Shin, N., Bhatia, S.K., Jeon, J.-M., Yoon, J.-J., Yoo, J., Ahn, J., et al., 2023. Polyhydroxybutyrate production from crude glycerol using a highly robust bacterial strain halomonas sp. YLGW01. Int. J. Biol. Macromol. 236, 123997.

Kumar, S.B., Moslemian, D., Duduković, M.P., 1997. Gas-holdup measurements in bubble columns using computed tomography. AIChE J 43, 1414–1425.

Kumar, M., Rathour, R., Singh, R., Sun, Y., Pandey, A., Gnansounou, E., Andrew Lin, K.-Y., Tsang, D.C.W., Thakur, I.S., 2020. Bacterial polyhydroxyalkanoates: opportunities, challenges, and prospects. J. Clean. Prod. 263, 121500.

Lee, H.-J., Kim, S.-G., Cho, D.-H., Bhatia, S.K., Gurav, R., Yang, S.-Y., Yang, J., Jeon, J.-M., Yoon, J.-J., Choi, K.-Y., et al., 2022. Finding of novel lactate utilizing bacillus sp. YHY22 and its evaluation for polyhydroxybutyrate (PHB) production. Int. J. Biol. Macromol. 201, 653–661.

Levett, I., Birkett, G., Davies, N., Bell, A., Langford, A., Laycock, B., Lant, P., Pratt, S., 2016. Techno-economic assessment of poly-3-hydroxybutyrate (PHB) production from methane—the case for thermophilic bioprocessing. J. Environ. Chem. Eng. 4, 3724–3733.

Liu, L.-Y., Xie, G.-J., Xing, D.-F., Liu, B.-F., Ding, J., Ren, N.-Q., 2020. Biological conversion of methane to polyhydroxyalkanoates: current advances, challenges, and perspectives. Environ. Sci. Ecotechnology 2, 100029.

López, J.C., Arnáiz, E., Merchán, L., Lebrero, R., Muñoz, R., 2018. Biogas-based polyhydroxyalkanoates production by methylocystis hirsuta: a step further in anaerobic digestion biorefineries. Chem. Eng. J. 333, 529–536.

Mavaddat, P., Mousavi, S.M., Amini, E., Azargoshasb, H., Shojaosadati, S.A., 2014. Modeling and CFD-PBE simulation of an airlift bioreactor for PHB production. Asia Pac. J. Chem. Eng. https://doi.org/10.1002/apj.1785.

Mohan T.R., Kumar, M.S.M., Rao, L., 2021. Numerical modelling of oxygen mass transfer in diffused aeration systems: A CFD-PBM approach. J. Water Process Eng. 2021, 40: 101920.

Moradi, Rashedi, Mofradnia, Khosravi-Darani, Ashouri, Yazdian, 2019. Polyhydroxybutyrate production from natural gas in A bubble column bioreactor: simulation using COMSOL. Bioengineering 2019, 6:84.

Mühlbauer, A., Hlawitschka, M.W., Bart, H., 2019. Models for the numerical simulation of bubble columns: a review. Chem. Ing. Tech. 91, 1747–1765.

Myung, J., Galega, W.M., Van Nostrand, J.D., Yuan, T., Zhou, J., Criddle, C.S., 2015. Long-term cultivation of a stable methylocystis -dominated methanotrophic enrichment enabling tailored production of poly(3-hydroxybutyrate-co-3-hydroxyvalerate). Bioresour. Technol. 198, 811–818.

Ngo, S.I., Lim, Y.-I., 2020. Multiscale eulerian CFD of chemical processes: a review. Chem Eng. 4, 23.

Painmanakul, P., Wachirasak, J., Jamnongwong, M., Hébrard, G., 2009. Theoretical prediction of volumetric mass transfer coefficient (kLa) for designing an aeration tank. Eng J. 13, 13–28.

Reilly, I.G., Scott, D.S., Debruijn, T.J.W., Macintyre, D., 1994. The role of gas phase momentum in determining gas holdup and hydrodynamic flow regimes in bubble column operations. Can. J. Chem. Eng. 72, 3–12.

Rodríguez, Y., Firmino, P.I.M., Pérez, V., Lebrero, R., Muñoz, R., 2020. Biogas valorization via continuous polyhydroxybutyrate production by methylocystis hirsuta in a bubble column bioreactor. Waste Manage. 113, 395–403.

Rodríguez, Y., García, S., Lebrero, R., Muñoz, R., 2023. Continuous polyhydroxybutyrate production from biogas in an innovative two-stage bioreactor configuration. Biotechnol. Bioeng. https://doi.org/10.1002/bit.28507.

Rostkowski, K.H., Pfluger, A.R., Criddle, C.S., 2013. Stoichiometry and kinetics of the PHB-producing type II methanotrophs methylosinus trichosporium OB3b and methylocystis parvus OBBP. Bioresour. Technol. 132, 71–77.

Schiller, L., Naumann, Z., 1933. Über die grundlegenden berechnungen bei der schwerkraftbereitung. Zeitschrift Des Vereines Deutscher Fngenieure 77, 318–321.

Schügerl, K., Lücke, J., Oels, U., 2006. **Bubble column bioreactors**. Adv. Biochem. Eng. 7. Springer-Verlag; 2006:1–84.

Shi, W., Yang, J., Li, G., Zong, Y., Yang, X., 2020. Computational fluid dynamics-population balance modeling of gas-liquid two-phase flow in bubble column reactors with an improved breakup kernel accounting for bubble shape variations. Heat Transfer Eng. 41, 1414–1430.

Wang, Z., Guo, K., Liu, H., Liu, C., Geng, Y., Lu, Z., Jiao, B., Chen, D., 2020. Effects of bubble size on the gas–liquid mass transfer of bubble swarms with sauter mean diameters of 0.38–4.88 mm in a co-current upflow bubble column. J. Chem. Technol. Biotechnol. 95, 2853–2867.

Wang, K., Hobby, A.M., Chen, Y., Chio, A., Jenkins, B.M., Zhang, R., 2021. Techno-economic analysis on an industrial-scale production system of polyhydroxyalkanoates (PHA) from cheese by-products by halophiles. Processes 10, 17.

Wendlandt, K.-D., Jechorek, M., Helm, J., Stottmeister, U., 2001. Producing poly-3-hydroxybutyrate with a high molecular mass from methane. J. Biotechnol. 86, 127–133.